Surface Formation of Nano- / Micro- Structures on Titanium Alloy Composites using Picosecond Laser Scanning Technology

Yi-Cheng Lin, Chih-Chung Yang, Shih-Feng Tseng, Donyau Chiang, Yu-Hsuan Lin, Kuo-Cheng Huang and Wen-Tse Hsiao
Instrument Technology Research Center, National Applied Research Laboratories, 20, R&D Rd. VI. Hsinchu Science Park, Hsinchu City, Taiwan

Keywords: Laser Fluence, Laser Material Interaction, Nano- / Micro Surface Structure Formation.

Abstract: This study reports on the development of picosecond laser system to titanium alloy surface treatment applications. In the picosecond laser-scanning system, that is based on the fiber-optics laser source and integrated with a designed optics / optical machine design and control technology of scanning system. To analyze the laser material interaction, the laser fluence, pulse repetition frequency of laser source, position of focused points, scan speed and pulse duration were adjusted. After laser surface treatment, the surface roughness and surface morphologies of treated surface were evaluated by using a field emission scanning electron microscope. Moreover, the contact angle measurement was used to analyze the hydrophilic and hydrophobic properties of the treatment surface with micro- / nano- structures.

1 INTRODUCTION

Titanium alloy is a strong, anti-corrosive, elastic, heat-resistant, cold-resistant, highly biocompatible, lowly thermally conductive, and non-magnetic material often used in medical supplies. It can be implanted in vivo to bind to tissue, whose functions are thus enhanced. The surface of titanium alloy can be modified to enhance its biocompatibility, bacterial resistance, surface lubrication, wetness, durability, corrosion resistance, and service life, as well as minimize its friction with the tissue. Common surface modification processes include ion beam treatment and ultraviolet curing, such as surface absorption, drug sequestering, ion-assisted deposition, ion implantation, and physical vapor deposition. Ultrafast lasers has many properties, during interaction processing, the ultrafast laser pulses do not deposit heat in material, the absorption process in the material can happen via multiphoton absorption if the intensity is high enough. Therefore, they can be used to fabricate microstructures or nanostructures on various materials through laser-material interaction. (Katahira et al., 2016) developed the laser-induced surface treatment in calcium nitrate solution conditions for improving the biocompatibility of titanium alloys using Yb fiber pulse laser. (Shen et al., 2017) proposed multi impact laser shock processing on an orthopaedic Ti-6Al-7Nb that can enhance the sliding wear and microhardness by 44 % and 22 %, respectively. (Kuczyńska et al., 2016) used direct laser interference lithography method to produce a periodic structure on titanium surface using two-channel Q-switched Nd:YAG laser. According to the laser surface treatment, the created roughness were ranged from nano- to micro- meters. (Huerta-Murillo et al., 2017) presented two laser micro-machining techniques (i.e. based on nanosecond direct Laser writing and picosecond direct laser interference patterning) on Ti-6Al-4V alloy. By using the static contact angle measurements were made to analyze the wettability behavior of the structures. Experimental results indicated that a hydrophobic behavior for the hierarchical structures. (Oliveira et al., 2009) fabricated microscale/nanoscale periodic and aperiodic structures on titanium using a pulse laser between 0.5 and 2 J/cm^2. The researchers found that the outward diffusion of laser energy produced periodic shockwaves and that different scan speeds produced different periodic shockwave structures. Subsequently different periodic microstructures and nanostructures were fabricated when the laser energy was lower than the threshold of the material removal. (Angéline et al., 2011)

Lin, Y-C., Yang, C-C., Tseng, S-F., Chiang, D., Lin, Y-H., Huang, K-C. and Hsiao, W-T.
Surface Formation of Nano- / Micro- Structures on Titanium Alloy Composites using Picosecond Laser Scanning Technology.
DOI: 10.5220/0006614201900196
In *Proceedings of the 6th International Conference on Photonics, Optics and Laser Technology (PHOTOPTICS 2018)*, pages 190-196
ISBN: 978-989-758-286-8

adopted a laser surface processing method to fabricate microstructures on cast titanium alloy and analyzed the mechanical properties of these structures. The researchers used an Nd:YAG laser and argon as the protective gas. Scanned electron microscopy, X-ray diffraction (XRD), atomic emission spectrometry, stretching tests, and hardness tests were performed for analyses. XRD outcomes showed significant TiO_2 and Ti_2N peaks when argon was absent. A significantly smaller TiO_2 peak and no Ti_2N peak were exhibited with the application of argon. (Coelho et al., 2011) analyzed the biomechanical performance of three implant surface processing methods and found that favorable biocompatibility was achieved in both the 14-day and 40-day tests. (Bereznai et al., 2003) modified the surface of titanium alloy implant materials using a subpicosecond (0.5 ps) argon fluoride (ArF) excimer laser to enhance biocompatibility after implantation and fabricate surface with different roughness levels to reduce surface tarnish. (Yoshinari et al. 2011) applied different surface chemical processing methods to achieve quantitative surface bond strength. The researchers analyzed the surface/section morphology of the implants and the materials adhered to the implants and validated that surface roughness was a key factor affecting the implants. Biological compatibility of titanium alloy materials are determined by the properties of the thin film after surface processing. Surface modification can improve the compatibility between implants and organic tissue. (Elias et al., 2008) introduced a method to examine surface morphology and surface roughness of processed materials. The method serves as a tool for in-depth research into titanium alloy implant materials. (Serap et al., 2012) used a nanosecond (200-250 ns) fiber laser (1060 nm) to scan and process the surfaces of four different titanium alloy structures and obtain different surface morphology and surface roughness data. Empirical results indicated that honeycomb-shaped surface structures facilitated future implant manifestation. (Milovanović et al., 2013) used a KrCl (222 nm) laser and a XeCl (308 nm) laser to modify the surface of titanium alloy material (Ti-6Al-4V). Test and analysis results showed that the XeCl laser achieved a rougher surface and higher removal rate than the KrCl laser. Post-modification oxidation conditions suggested that excimer lasers with longer wavelengths are more likely to cause oxidation on the surface of titanium alloy, roughly 5-8 times more likely than lasers with short wavelengths.

In this study, a picosecond laser scanner was adopted to modify the surface of titanium alloy materials and explore laser-material interaction and the formation of nanoscale and microscale structures. Field-emission SEM (FE-SEM) was used to analyze the microstructures of the modified materials, specifically, surface roughness and morphology. In addition, a contact angle meter was used to measure the surface hydrophilicity/hydrophobicity of the nanostructures and microstructures.

2 PICOSECOND PULSED LASER SCANNING SYSTEM

The picosecond ultrafast laser scanner comprises an optical configuration, expanded beam collimator, reflectors, scanner, and a human-machine interface for system control. The laser beam passes into the collimator via the first reflector and into the scanner. The scanner focuses the beam on the titanium alloy for surface modification. The layout of the picosecond laser scanner is illustrated in Figure 1. The specifications of the picosecond ultrafast laser scanner are tabulated in Table 1.

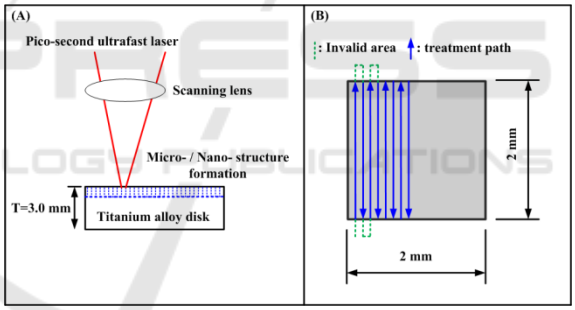

Figure 1: Schematic diagram of the picosecond laser scanning system.

Table 1: Specification of the picosecond laser scanning system.

Item	Parameters
Pulse repetition frequency (kHz)	~1000
Average power (watt)	~14
Laser mode	TEM_{00} (M^2<1.4)
Laser pulse width (FHWM, ps)	<15

2.1 Laser Fluence Calculation

In the laser processing, pulse width refers to the amount of time required for a single laser beam to apply a specific number of shots on the workpiece. Energy density increases concurrently with a decrease in pulse width, and the absorption energy on the surface of the workpiece depends on the

output power and irradiation time of the laser. Moreover, the irradiation time of continuous-pulse laser beams is attributed to scan speed, while that of single-pulse laser beams is attributed to pulse width. Therefore, the energy absorbed by the material increases concurrently with power. The laser fluence depended on the average laser power, pulse width and operation pulse frequency, respectively. In this study, assuming that the average output power of a laser is (P_a) and that pulse width affects instantaneous power (P_p), the following equation can be expressed:

$$P_p = \left(\frac{P_a}{\Delta T} \right) \quad (1)$$

$$\Delta T = PRF \times t \quad (2)$$

$$P_p = \left(\frac{P_a}{PRF \times t} \right) \quad (3)$$

$$E_l = P_p \times t \quad (4)$$

where, P_p (W) is instantaneous power, P_a (W) is average power, and ΔT is the product of single-pulse irradiation time and repeat frequency, as expressed in Eq. (2). ΔT can be incorporated into Eq. (1) to derive Eq. (3). Laser fluence (E_l) can be calculated using Eq. (4).

2.2 Wettability Characteristics and Contact Angle Evaluation

By using the droplet experiments analysis were carried out the wettability behavior of the surface formation. For the contact angle measurement, the droplet shapes were captured by a FTA 188 video contact angle analyzer. In the contact angle evaluation, (Young 1805) analyzed the contact angle (θc) of droplets, as illustrated in Figure 2. Contact angle can be calculated using Eq. (5).

$$\gamma_{SG} = \gamma_{SL} + \gamma_{LG} \cos\theta \quad (5)$$

where, γ_{SG}, γ_{SL}, and γ_{LG} represent the surface tension between a solid and gas, between a solid and a liquid, and between a liquid and gas, respectively.

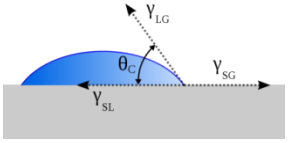

Figure 2: Schematic diagram of the contact angle evaluation.

When the contact surface with rough surface, the contact angle becomes θ_{W*}, by (Wenzel 1936) as illustrated in Figure 3 (middle). The contact angle can be calculated using Eq. (6).

$$\cos\theta_{W*} = r\cos\theta \quad (6)$$

where, r is the projected area to the actual area. Equation (6) indicates that the surface of the microstructures increases surface tension. Hydrophobic surfaces (θ > 90°) become more hydrophobic when they contain microstructures, and hydrophilic surfaces (θ < 90°) become more hydrophilic when they contain microstructures. Subsequently, the contact angles are smaller with microstructures than without microstructures, as illustrated in Figure 3.

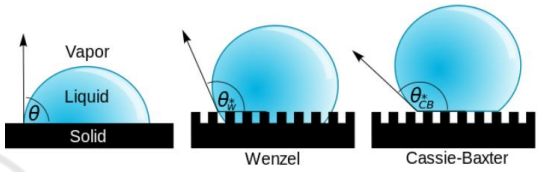

Figure 3: Schematic diagram of the contact angle under different microstructures.

When the contact surface with microstructure, (Cassie and Baxter 1945) found that the contact angle at which liquid suspended on the surface of microstructures became θ_{CB*}, as illustrated in Fig. 3 (right). Subsequently, θ_{CB*} can be calculated using Eq. (7). Therefore, Eq. (8) must be true if the Cassie-Baxter condition exists.

$$\cos\theta_{CB*} = \varphi(\cos\theta + 1) - 1 \quad (7)$$

$$\cos\theta < (\varphi - 1)/(r - \varphi) \quad (8)$$

where φ is the fraction of the solid–liquid interface below the drop.

3 TITANIUM ALLOY SURFACE MODIFICATION USING PICOSECOND ULTRAFAST LASER SCANNING

To obtain different surface modification outcomes (incl., surface morphology and nanostructures and microstructure properties and dimensions), tests were performed with fluence settings of 5, 10, 15, 20, and 25 μJ and a pulse time settings of 25, 50, 100, 200, and 500 μs (Figure. 4).

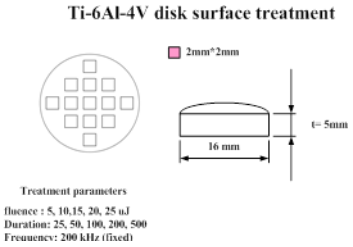

Figure 4: Experiment parameter planning of ultrafast laser surface treatment on Ti-6Al-4V alloys disk.

3.1 Surface Morphology and Nanostructure and Microstructure Properties and Dimensions of Modified Titanium Alloy

A sample of a titanium ingot (ψ=12.7 mm/t=3-5 mm) modified using a picosecond ultrafast laser is illustrated in Figure 5. In the figure, the pulse time settings were 25, 50, 100, 200, and 500 μs from left to right, and the fluence settings were 5, 10, 15, 20, and 25 μJ from top to bottom.

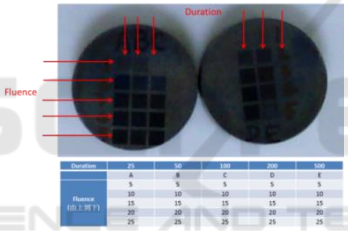

Figure 5: Experiment results of ultrafast laser surface treatment Ti-6Al-4V disk.

An FE-SEM was performed to analyze the surface microstructures (Figure 6). Observations were as follows:

(a) Fixed pulse time of 25 μs (Figure 6(a-1)-(a-10)): No periodic structures were observed on the modified surface at a fluence setting of 5 μJ. Periodic structures with a pitch of roughly 500 nm were observed when at fluence settings of 10, 15, 20, and 25 μJ. No obvious nanoparticles were observed on the structures at a fluence setting of 10 μJ. Obvious nanoparticles (roughly 100-300 nm) were observed at fluence settings of 15, 20, and 25 μJ. However, the size of the nanoparticles decreased concurrently with an increase in laser fluence.

(b) Fixed pulse time of 50 μs (Figure 6(b-1)-(b-10)): No periodic structures were observed on the modified surface at a fluence setting of 5 μJ. Periodic structures with a pitch of roughly 500 nm were observed when at fluence settings of 10, 15, 20, and 25 μJ. Obvious nanoparticles were observed on the structures at a fluence setting of 10 μJ (~100 nm). Obvious nanoparticles (roughly 200-300 nm) were observed at fluence settings of 15, 20, and 25 μJ. However, the size of the nanoparticles decreased concurrently with an increase in laser fluence (200-300 nm).

(c) Fixed pulse time of 100 μs (Figure 6(c-1)-(c-10)): No periodic structures were observed on the modified surface at a fluence setting of 5 μJ. However, flaky lines were observed. Slightly obvious periodic and filamentary structures were observed at a fluence setting of 10 μJ. Periodic structures with a pitch of roughly 500 nm were observed when at fluence settings of 10, 15, 20, and 25 μJ. Obvious nanoclusters (~300 nm) were observed on the periodic structures. However, the nanoclusters decreased concurrently with an increase in laser fluence (300 nm-100 nm).

(d) Fixed pulse time of 200 μs (Figure 6(d-1)-(d-10)): No periodic structures were observed on the modified surface at a fluence setting of 5 μJ. No obvious periodic microstructures and nanostructures were observed at a fluence setting of 10 μJ. The structures were largely remelting structures. No obvious periodic microstructures and nanostructures were observed at a fluence setting of 15 μJ. The structures were largely remelting structures with a pore size of 20-30 nm. No obvious periodic microstructures and nanostructures were observed at a fluence setting of 20 μJ. The structures were largely remelting structures with a pore size of 200 nm. No obvious periodic microstructures and nanostructures were observed at a fluence setting of 25 μJ. The structures were largely remelting structures with a pore size of 50 nm. These observations show that the structures produced at this pulse time setting were porous remelting structures. No obvious periodic structures were produced.

(e) Fixed pulse time of 500 μs (Figure 6(e-1)-(e-10)): No periodic structures were observed on the modified surface at a fluence setting of 5 μJ. The structures were largely remelting structures. Obvious periodic microstructures and nanostructures with a pitch of 500 nm were observed at a fluence setting of 10 μJ. Obvious remelting structures with a pore size of ~100 nm were observed at a fluence setting of 15 μJ. Obvious remelting structures with a pore size of ~50 nm were observed at a fluence setting of 20 μJ. Obvious remelting structures with a pore size of 20-30 nm were observed at a fluence setting of 25 μJ.

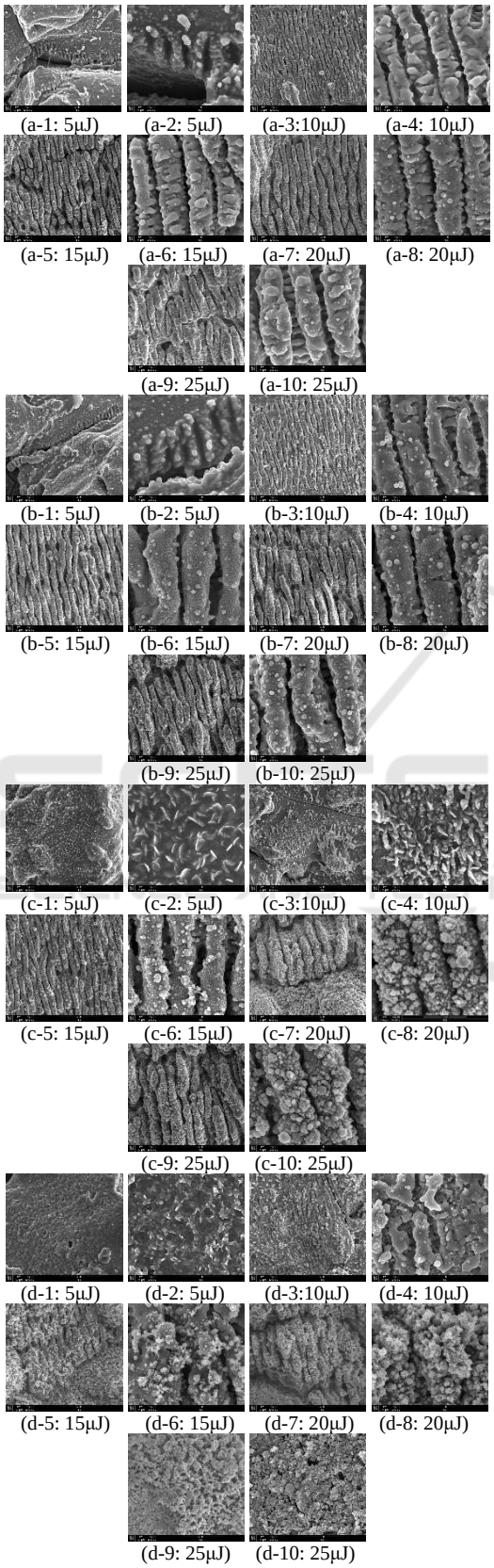

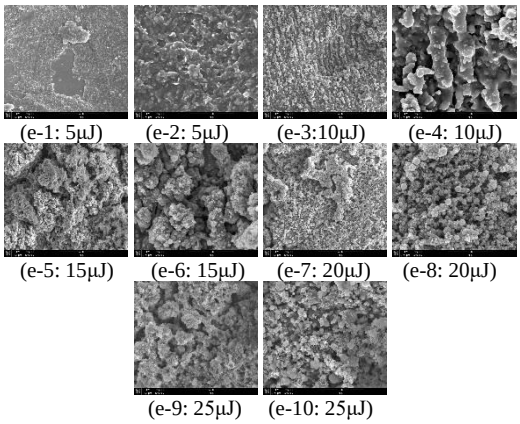

Figure 6: SEM images of the nano- / micro- structure morphologies on ultrafast laser surface treatment Ti-6Al-4V disk. (a) 25μs, (b)50μs, (c)100μs, (d)200μs, (e)500μs.

3.2 Contact Angle Measurement of Modified Titanium Alloy

The contact angle of the original (unprocessed) specimen was 90.66°. The measurement curve of the contact angle of the modified specimen is illustrated in Figure 7. The pulse time settings were increased in increments from 50 to 500 μs at fixed fluence settings of 5, 10, and 15 μJ. The contact angle increased concurrently with pulse time, forming hydrophobic structures. However, the contact angle decreased concurrently with an increase in pulse time when fluence was increased from 20 to 25 μJ. Hydrophilic structures were observed when the settings were 20 μJ/500 μs and 25 μJ/500 μs.

A comparison of the structures illustrated in Figure 6 revealed that the dimensions of the nanostructures and microstructures affected the specimen's moisture and droplet-catching ability. The nanostructures and microstructures fabricated at all fluence settings and at pulse time settings of 25 and 50 μs achieved a contact angle of >120°.

A contact angle of >140° can be achieved under appropriate fluence/pulse time combinations. The parameters and outcomes were: (a) 25 μJ / 25 μs / 141.6°, (b) 20 μJ / 25 μs / 151.4°, (c) 15 μJ / 200 μs / 159.07°, and (d) 10 μJ / 25 μs / 143.98°.

At a fixed fluence setting of 5 μJ, the contact angle peaked at 132.26° (@50 μs). However, remelting occurred as pulse time increased, replacing periodic structures with hydrophilic structures.

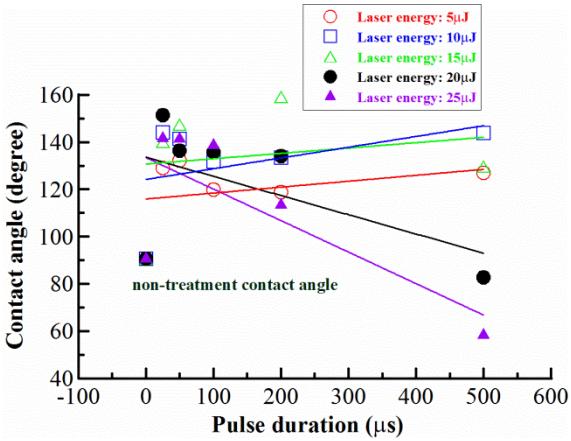

Figure 7: Contact angle measurement results of ultrafast laser surface treatment Ti-6Al-4V disk.

4 CONCLUSIONS

In this study, a picosecond laser scanner was successfully used to modify the surface of titanium alloy.

An experimental analysis was performed to elucidate the factors affecting periodic structures, including pulse time and fluence, and the effects that these factors have on periodic nanostructures and microstructures and the hydrophilicity/hydrophobicity of contact angles. Analysis outcomes were as follows:

(a) A picosecond laser scanner was used to modify the surface of a titanium ingot (ψ=12.7 mm/t=3-5 mm). Nanoscale and microscale periodic structures were observed on the modified surface. The structures were parallel to the scanning direction (S) and perpendicular to the electric field direction (E). The pitch of the periodic structures was roughly 500 nm.

(b) At a fixed pulse time setting of 25 μs, obvious nanoparticles (roughly 100-300 nm) were observed at fluence settings of 15, 20, and 25 μJ. However, the size of the nanoparticles decreased concurrently with an increase in laser fluence (300-100 nm).

(c) At a fixed pulse time setting of 50 μs, obvious nanoparticles (200-300 nm) were observed at fluence settings of 15, 20, and 25 μJ. However, the size of the nanoparticles decreased concurrently with an increase in laser fluence (200-300 nm).

(d) At a fixed pulse time setting of 100 μs, slightly obvious periodic and filamentary structures were observed at a fluence setting of 10 μJ. Periodic structures with a pitch of roughly 500 nm were observed when at fluence settings of 10, 15, 20, and 25 μJ. Obvious nanoclusters (~300 nm) were observed on the periodic structures. However, the nanoclusters decreased concurrently with an increase in laser fluence (300 nm-100 nm).

(e)At a fixed pulse time setting of 200 μs, no obvious periodic microstructures and nanostructures were observed at a fluence setting of 10 μJ. The structures were largely remelting structures. No obvious periodic microstructures and nanostructures were observed at a fluence setting of 15 μJ. The structures were largely remelting structures with a pore size of 20-30 nm. No obvious periodic microstructures and nanostructures were observed at a fluence setting of 20 μJ. The structures were largely remelting structures with a pore size of 200 nm. No obvious periodic microstructures and nanostructures were observed at a fluence setting of 25 μJ. The structures were largely remelting structures with a pore size of 50 nm. These observation show that the structures produced at this pulse time setting were porous remelting structures. No obvious periodic structures were produced.

(f) At a fixed pulse time setting of 500 μs, no periodic structures were observed on the modified surface at a fluence setting of 5 μJ. The structures were largely remelting structures. Obvious periodic microstructures and nanostructures with a pitch of 500 nm were observed at a fluence setting of 10 μJ. Obvious remelting structures with a pore size of ~100 nm were observed at a fluence setting of 15 μJ. Obvious remelting structures with a pore size of ~50 nm were observed at a fluence setting of 20 μJ. Obvious remelting structures with a pore size of 20-30 nm were observed at a fluence setting of 25 μJ.

(g) The contact angle of the hydrophobic structures fabricated on the surface of the modified material peaked at 159.07° (@15 μJ/200 μs). Excessive pulse time and fluence settings (@20 μJ/500 μs and @25 μJ/500 μs) caused the contact angle to drop below that of the unprocessed material (90.66°), forming hydrophilic structures. The reason for the reduction in contact angle was because of the occurrence of remelting as pulse time increased, replacing periodic structures with hydrophilic structures.

ACKNOWLEDGEMENTS

This work was supported in part by the Ministry of Science and Technology, TAIWAN, numbers MOST 104-2622-E-492-0008-CC3.

REFERENCES

Katahira, K., Ezura, A., Ohkawa, K., Komotori, J., Ohmori, H., 2016. Generation of biocompatible titanium alloy surfaces by laser-induced wet treatment. *CIRP Ann. Manuf. Techn.*, Vol. 65, pp. 237-240.

Shen, X., Shukla, P., Nath, S., Lawrence, J., 2017. Improvement in mechanical properties of titanium alloy (Ti-6Al-7Nb) subject to multiple laser shock peening. *Surf. Coat. Technol.*, Vol. 327, pp. 101-109.

Kuczyńska, D., Kwaśniak, P., Marczak, J., Bonarski, J., Smolik, J., Garbacz, H., 2016. Laser surface treatment and the resultant hierarchical topography of Ti grade 2 for biomedical application. *Appl. Surf. Sci.*, Vol. 390, pp.560-569.

Huerta-Murillo, D., Aguilar-Morales, A.I., Alamri, S., Cardoso, J.T., Jagdheesh, R., Lasagni, A.F., Ocaña, J.L., 2017. Fabrication of multi-scale periodic surface structures on Ti-6Al-4V by direct laser writing and direct laser interference patterning for modified wettability applications. *Opt. Lasers Eng.*, Vol. 98, pp.134-142.

Oliveira, V., Ausset, S., Vilar, R., 2009. Surface micro/nanostructuring of titanium under stationary and non-stationary femtosecond laser irradiation. *Appl. Surf. Sci.*, Vol. 255, pp. 7556-7560.

Angéline, P.Q., Ikuya, W., Etsuko W., Caroline B., 2011. Microstructure and mechanical properties of surface treated cast titanium with Nd:YAG laser. *Dent. Mater.*, Vol. 28, pp. 945-951.

Coelho, P.G., Granato, R., Marin, C., Teixeira, H.S., Suzuki, M., Valverde, G.B., Janal, M.N., Lilin, T., Bonfante, E.A., 2011. The effect of different implant macrogeometries and surface treatment in early biomechanical fixation: An experimental study in dogs. *J. Mech. Behav. Biomed. Mater.*, Vol. 284, pp. 1974-1981.

Bereznai, M., Pelsöczi, I., Tóth, Z., Turzó, K., Radnai, M., Bor, Z., Fazekas, A., 2003. Surface modifications induced by ns and sub-ps excimer laser pulses on titanium implant material. *Biomaterials*, Vol. 24, pp. 4197-4203.

Yoshinari, M., Matsuzaka, K., Inoue, T., 2011. Surface modification by cold-plasma technique for dental implants– Bio-functionalization with binding pharmaceuticals. Jpn. Dent. Sci. Rev., Vol. 47, pp. 89-101.

Elias, C.N., Oshida, Y., Lima, J.H.C., Muller, C.A., 2008. Relationship between surface properties (roughness, wettability and morphology) of titanium and dental implant removal torque. *J. Mech. Behav. Biomed. Mater.*, Vol. 23. pp. 234-242.

Serap, C., Hüseyin Ö., 2012. Laser-induced novel patterns: As smart strain actuators for new-age dental implant surfaces. *Appl. Surf. Sci.*, Vol. 263, pp. 579-585.

Milovanović, D.S., Petrović, S.M., Shulepov, M.A., Tarasenko, V.F., Radak, B.B., Miljanić, Š.S., Trtica, M.S., 2013. Titanium alloy surface modification by excimer laser irradiation. *Opt. Laser Technol.*, Vol. 54, pp. 419-427.

Young, T., 1805. An Essay on the Cohesion of Fluids. *Phil. Trans. R. Soc. Lond.*, Vol. 95, pp. 65-87.

Wenzel, RN., 1936. Resistance of Solid Surfaces to Wetting by Water. *Ind. Eng. Chem.*, Vol. 28m pp. 988-994.

Cassie, A.B.D., Baxter, S., 1945. The water repellency of fabrics and a new water repellency test. *Tex. Inst. J.*, Vol. 36, pp. 67-90.